Lab on a Chip

PAPER

View Article Online
View Journal

Check for updates

Cite this: DOI: 10.1039/c8lc00255j

Splitting and separation of colloidal streams in sinusoidal microchannels†

Mathias Schlenk,[a] Markus Drechsler,[ab] Matthias Karg,[c] Walter Zimmermann,[d] Martin Trebbin *[e] and Stephan Förster *[af]

Received 10th March 2018,
Accepted 30th August 2018

DOI: 10.1039/c8lc00255j

rsc.li/loc

The control of the distribution of colloidal particles in microfluidic flows plays an important role in biomedical and industrial applications. A particular challenge is to induce cross-streamline migration in laminar flows, enabling the separation of colloidal particles according to their size, shape or elasticity. Here we show that viscoelastic fluids can mediate cross-streamline migration of deformable spherical and cylindrical colloidal particles in sinusoidal microchannels at low Reynolds numbers. For colloidal streams focused into the center of the channel entrance this leads to a symmetric stream-splitting and separation into four substreams. The degree of stream splitting and separation can be controlled *via* the flow rates, viscoelasticity of the focusing fluid, and the spatial microchannel modulation with an upper limit when reaching the microchannel walls. We demonstrate that this effect can be used to separate flexible particles of different size and shape. This methodology of cross-stream migration has thus great potential for the passive separation of colloids and cells in microfluidic channels.

1. Introduction

The fundamental understanding and control of particle distribution and separation in micro flows plays an important role in many biomedical, environmental and industrial applications.[1,2] Microfluidic particle sorting can be achieved *via* a variety of methods that cause cross-streamline migration. One class are noninvasive methods, which rely on intrinsic hydrodynamic properties of micro flows and particle properties.[3] Widely employed examples for particle focusing are based on fluid inertia,[4–9] on viscoelastic effects[10] or deformability-selective particle sorting.[11–14]

It was demonstrated for the first time by Segre *et al.* that rigid particles can migrate to stable off-center positions in pipe flows.[4] Migration was driven by fluid inertia in the intermediate Reynolds number range ($\sim 1 < \mathrm{Re} < \sim 100$) and has been extensively used for particle sorting in Newtonian and viscoelastic fluids.[5–9] In contrast, deformable particles like vesicles, capsules or cells show cross-streamline migration already in the limit of Stokes flows at very small values of the Reynolds number. They migrate away from channel walls due to the lift force, as shown at first for Newtonian liquids.[15–17] When separated from the wall deformable particles can migrate further towards the center in Poiseuille flows, driven by the local shear gradient across the particles.[12–14] Both effects depend on the particle size and their deformability. In shear thinning fluids the center migration of soft particles may be reversed by shear thinning effects[18] or elastic lift forces.[19–22] In viscoelastic fluids several types of cross-stream line migration phenomena have been observed for rigid and soft particles.[3,10,18,23] For example, particle focusing and alignment was achieved over a range of small to medium flow rates to separate solid and deformable particles and cells.[24] A spatially varying flow-channel cross-section may lead to center-line focusing of rigid particles in Newtonian fluids[25] and non-Newtonian fluids[26,27] or to unusual and unexpected reorientations of anisotropic flexible particles in shear thinning fluids.[28]

So far viscoelastic cross-stream migration of anisotropic or extended chain-like structures has received little attention, although the separation of synthetic or biological macromolecules or anisotropic nanoparticles is an important research field. Thus, we investigated the flow behavior of anisotropic, semiflexible wormlike micelles under conditions that promote cross-stream migration. To control and amplify migration we used sinusoidally modulated microchannels and investigated the flow behavior using fluorescence-, polarization-, and confocal laser scanning-microscopy (CLSM). Streams of the micellar solutions were hydrodynamically focused into the

[a] Physical Chemistry I, University of Bayreuth, 95440 Bayreuth, Germany
[b] Bavarian Polymer Institute, University of Bayreuth, 95440 Bayreuth, Germany
[c] Physical Chemistry I, Heinrich-Heine-University, 40204 Düsseldorf, Germany
[d] Theoretical Physics I, University of Bayreuth, 95440 Bayreuth, Germany
[e] Centre for Ultrafast Imaging (CUI), University of Hamburg, 22761 Hamburg, Germany. E-mail: martin.trebbin@uni-hamburg.de; Tel: +49 40 8998 2613
[f] JNCS-1/ICS-1, Forschungszentrum Jülich, 52428 Jülich, Germany. E-mail: s.foerster@fz-juelich.de; Fax: +49 2461 61 2610; Tel: +49 2461 61 85161

† Electronic supplementary information (ESI) available: Detailed photo- and soft lithographical microchip fabrication, characterization of colloids, detailed flow profile analysis, rheological data. See DOI: 10.1039/c8lc00255j

center of the modulated microchannels at low Reynolds numbers using Newtonian and non-Newtonian fluids. We surprisingly discovered that the central stream symmetrically splits into four substreams that separate and further move towards the outer wall of the microfluidic channel with every passage through a channel modulation. We show that stream splitting and separation can be controlled *via* flow rates, microchannel geometries, and colloid shape as well as the rheological properties of the focusing fluid. We outline the underlying physical principles for the observed separation effect and furthermore demonstrate that this phenomenon can be generally used to separate colloidal and cellular particles according to their size.

2. Results and discussion

2.1 Splitting of colloidal streams by 2D-focusing with non-Newtonian fluids

For our study of the flow behavior of anisotropic colloids, in our case wormlike micelles, we used sinusoidal microchannels with a channel design that is shown schematically in Fig. 1A. An aqueous solution of wormlike micelles at a concentration of 1 wt% was focused by two aqueous side streams into an outlet channel that had periodic sinusoidal variations of the channel width. The wormlike micelles were formed by the self-assembly of poly(isoprene-*b*-ethylene oxide) block copolymers (PI–PEO), which spontaneously occurs when dissolving the block copolymer in water. The channel height (h = 100 μm) was the same for all channels. The channel width was w = 250 μm for the central and both side channels, and was identical to the average width of the sinusoidal outlet channel. A typical flow rate in the central and side channels were Q = 200 μL h^{-1} leading to a total flow rate of Q = 600 μL h^{-1} in the outlet channel. We were interested in how the central stream of wormlike micelles respond to spatially periodic flow modulation leading to extension and contraction. For this we labelled the wormlike micelles with a fluorescent dye (Nile red) to follow the focused stream in the sinusoidal outlet channel using fluorescence microscopy.

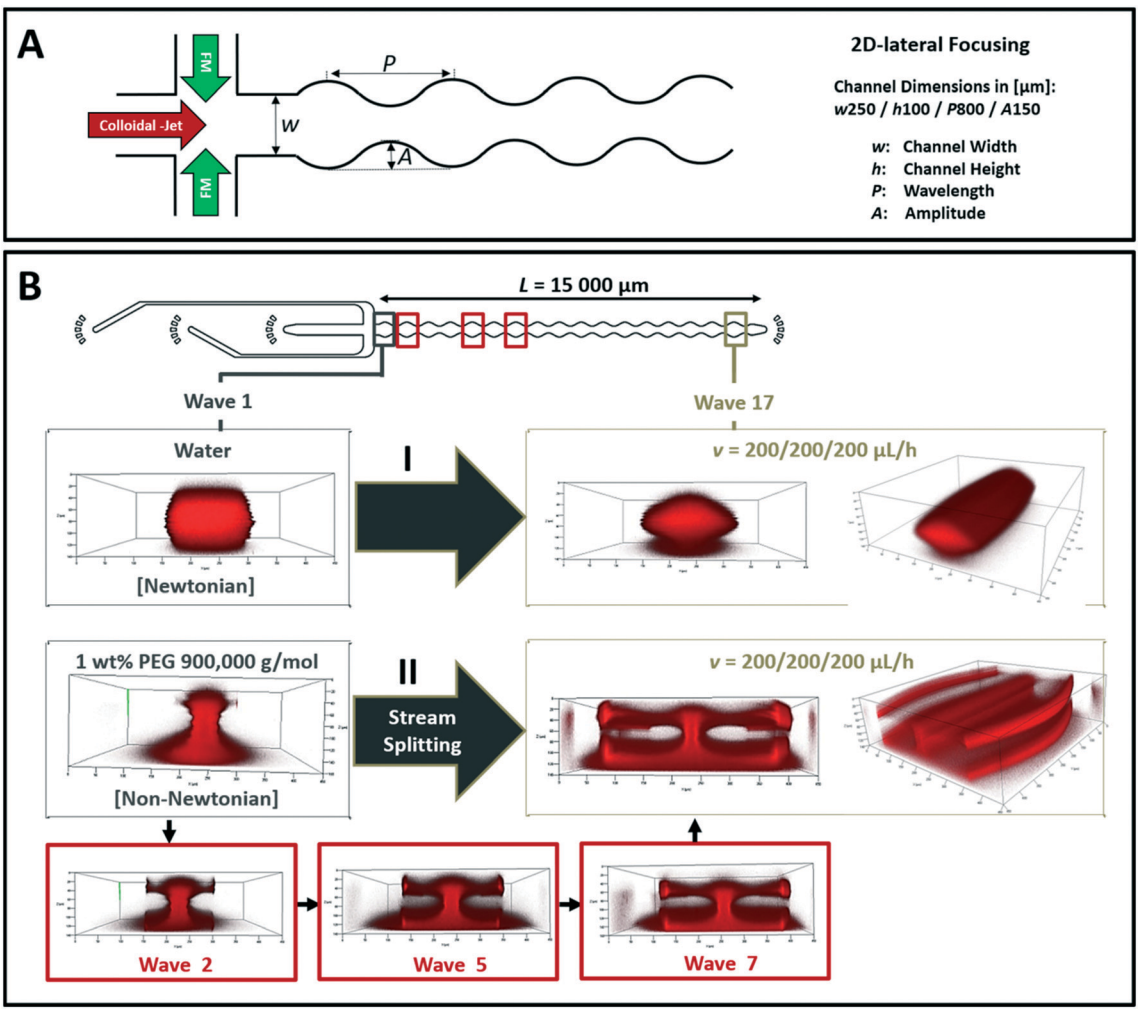

Fig. 1 (A) Scheme of the sinusoidal microchannel design with all parameter dimensions used for 2D-focusing. FM denotes the focusing medium. (B) 3D-CLSM front view images of Nile red labelled 1 wt% solutions of wormlike micelles which are hydrodynamically focused with water as a Newtonian fluid (I) and with a 1 wt% PEO-solution as a non-Newtonian fluid (II). The stream-splitting effect occurs near the microchannel floor and ceiling. The front view images of sine sections 2, 5 and 7 illustrate the subsequent increase of the stream-splitting with each sine section.

When using water as a focusing fluid we observed the expected periodic variation of the stream width, which expanded and contracted in proportion to the width of the outlet channel (Fig. 1B I). However, when using a non-Newtonian liquid for flow-focusing, we surprisingly discovered that the stream of wormlike micelles split into four substreams. This is shown in Fig. 1B II, where the confocal microscopy image on the left shows the central stream in the first sine section, where it is already slightly extended at the bottom and the floor of the channel. We always observe slight asymmetries between the floor and the ceiling layers in the microfluidic channel due to light scattering from the chip material, which increases from the cover slide and objective towards the center direction of the microfluidic chip device. The two confocal images on the right show the central stream in the 17th sine section, where it has split symmetrically into four substreams which are located close to the left and the right wall at the channel floor and channel ceiling. For flow-focusing we used a 1 wt% solution of a high molecular weight polyethylene glycol (PEG, 900 000 g mol^{-1}). Three additional images in Fig. 1B II show the increasing separation of the four streams in the 2nd, 5th, and 7th sine section. The part of the central stream that is located in the middle between the floor and the ceiling of the outlet channel does not split.

2.2 Influence of channel geometry

To clarify the conditions that lead to the splitting of the central stream, we compared a sinusoidal channel to a straight channel of the same total length of L = 1.5 cm, the same height of h = 100 μm, and the same average width w = 250 μm. The sinusoidal channel had a period of P = 800 μm and an amplitude of A = 150 μm. The results are presented in Fig. 2A I-a, which shows the CLSM side view and top view images. When using the 1 wt% PEG (900k)-solution for flow-focusing, for the straight channel the central stream width was 75 μm and did not change from the beginning to the end of the channel after 1.5 cm. When using the sine channel, the central stream with an original width of 75 μm splits into four substreams with a separation that increases by *ca.* 25 μm for each sine wave until the limit of h = 250 μm at the channel walls is finally reached. The increasing splitting and separation of the main stream at selected downstream positions is plotted in Fig. 2A 1-a.

Fig. 2A I-b shows the effect of the sine period and amplitude on the separation of the substreams. Decreasing each sine-period from P = 800 to 400 μm and increasing the amplitude from A = 150 to 300 μm lead to a considerably larger separation, *e.g.* from 200 to 350 μm at the 12th sine section. This demonstrates that the sine-form of the outlet channel is essential for the stream-splitting phenomenon and that by variation of the sine period and amplitude an efficient separation of the substreams can be accomplished over short outlet channel distances.

Next, we considered the influence of the channel floor and ceiling on the splitting of the central stream. To investigate this, we chose a 3D-focusing design such that the central stream was focused into the center of the outlet channel with considerable distance from the channel floor, ceiling and both side walls. The 3D-focusing channel design is schematically shown in Fig. 2B. The confocal microscopy images on the right in Fig. 2B clearly show that under these conditions we do not observe any splitting of the central stream. This suggests that the proximity of the channel floor and ceiling is necessary for the splitting and separation of the central stream.

2.3 Effect of molar mass, flow rate and other important parameters

High molecular weight polyethylene oxide (PEO)-solutions are non-Newtonian fluids that show pronounced shear-thinning. We therefore investigated PEOs of smaller molecular weights that show less pronounced shear thinning, eventually becoming near Newtonian at very low molecular weights. The measured flow-curves for each of the investigated polyethylene glycols are shown in the ESI† (Fig. S6A). The corresponding experiment with PEOs of different molecular weights were performed under standard conditions with a 1 wt% solution of wormlike micelles, a channel height h = 100 μm, an average channel width of w = 250 μm, a sine period of L = 800 μm, an amplitude of A = 150 μm, and a volumetric flow rate of Q = 600 μl h^{-1} in the outlet channel. In Fig. 3A CLSM-images of the central stream cross-sectional shapes in the first and the 17th sine section are compared for PEO-solutions with molecular weights of 6, 300, and 900 kg mol^{-1}. Whereas the 6 kg mol^{-1} low molecular weight PEO-solution showed no indications of stream splitting in the 17th sine section, the 300 kg mol^{-1} PEO-solution lead to a small, but clearly observable splitting. The 900 kg mol^{-1} PEO-solution lead to a very pronounced splitting of the central stream, as already described in Fig. 1 and 2. This indicates that the molecular weight of the polymer that is used in the focusing fluid must be sufficiently large to induce stream-splitting.

To investigate whether the observed stream splitting would be due to just a higher viscosity of the focusing stream compared to water, we also investigated glycerin as a Newtonian fluid which has a viscosity that is 1000 times larger compared to water. As visible in the ESI† (Fig. S6B), we did not observe any stream splitting with glycerin.

As for shear-thinning non-Newtonian fluids the solution viscosity depends on the shear rate, we investigated the splitting of the central stream for different flow velocities over a range of Q = 10–520 μl h^{-1}, corresponding to mean flow velocities of v = 0.1–6 mm s^{-1}. Front view CLSM images and top view fluorescence microscopy images of the streams at the last sine section of the channel are shown in Fig. 3B. There is no observable stream splitting at the lowest flow rate of 10 μl h^{-1}. At 80 μl h^{-1} we observe small but significant splitting,

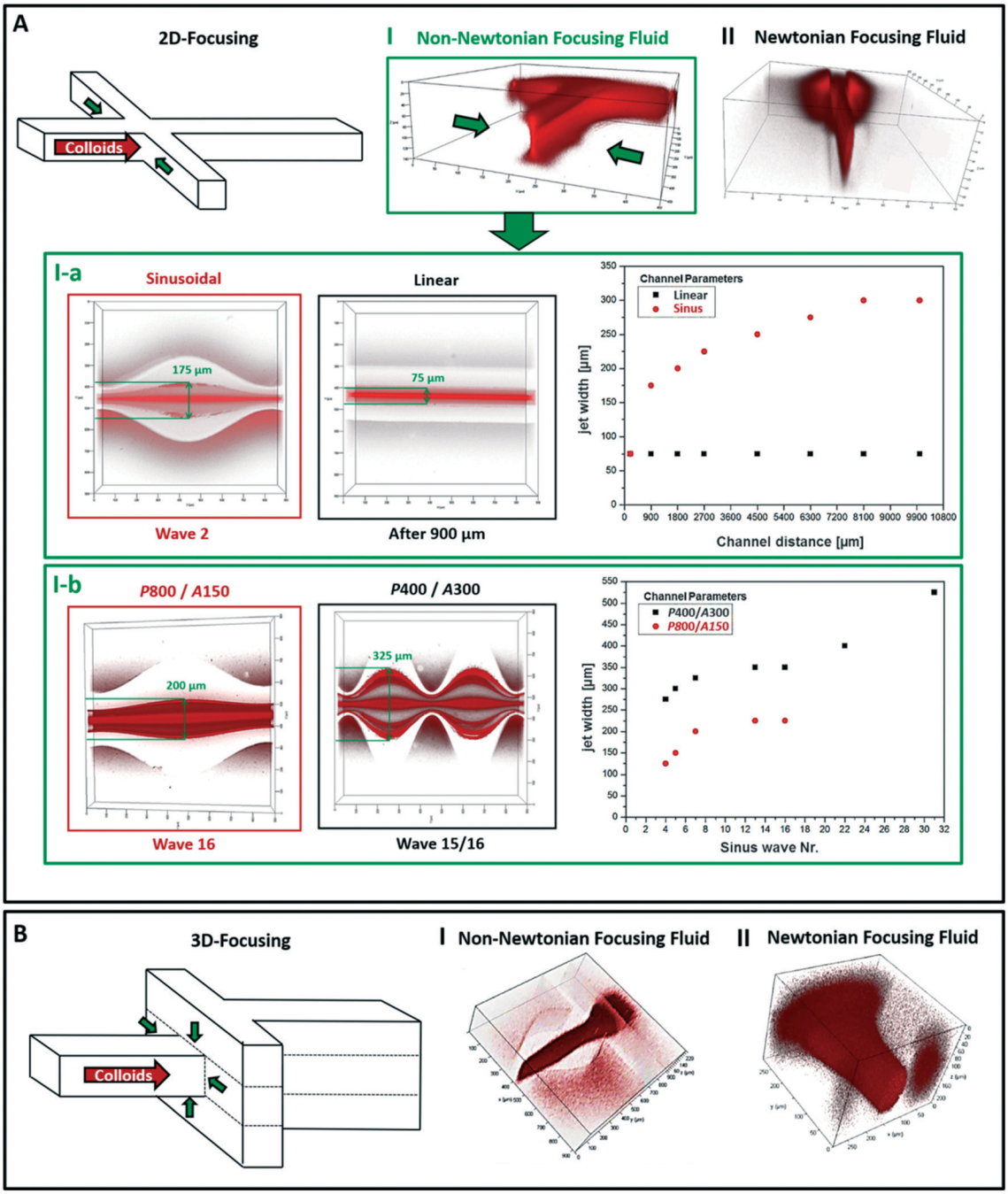

Fig. 2 (A) 3D-CLSM images of the arising stream-splitting effect by using 2D-focusing for a Nile red dyed 1 wt% wormlike micelles solution just in combination with non-Newtonian (I) and with Newtonian (II) focusing fluids. (I-a) Top view images of the stream-splitting in a sinus-shaped and a linear channel geometry as well as a comparative diagram concerning their sub-stream spreading distances. (I-b) Top view images of stream-splitting in sine-channels comparing half of the periodic wavelength P as well as double of the amplitude A and again a comparative diagram regarding their sub-stream spreading distances. (B) 3D-CLSM images of no emerging stream-splitting by applying a channel design with a 3D-focusing independent from using Newtonian (I) or non-Newtonian (II) focusing fluids.

which increases with increasing flow rate of up to 520 µl h^{-1}. Thus, also the flow velocity must be larger than a critical value to induce splitting of the central stream.

These experiments provide first indications on the conditions of the central stream splitting of wormlike micelles. The observation that splitting is observed at PEO molecular weights above ~300 kg mol^{-1} for concentrations of ~1 wt% indicates that the effect is related to the overlap concentration c^* of the polymer chains in solution. The PEO overlap concentration can be estimated using the known relation between the hydrodynamic radius and the molecular weight, $R_h = kM^{\alpha}$, where k = 0.0145 nm and α = 0.571,[29] an exponent

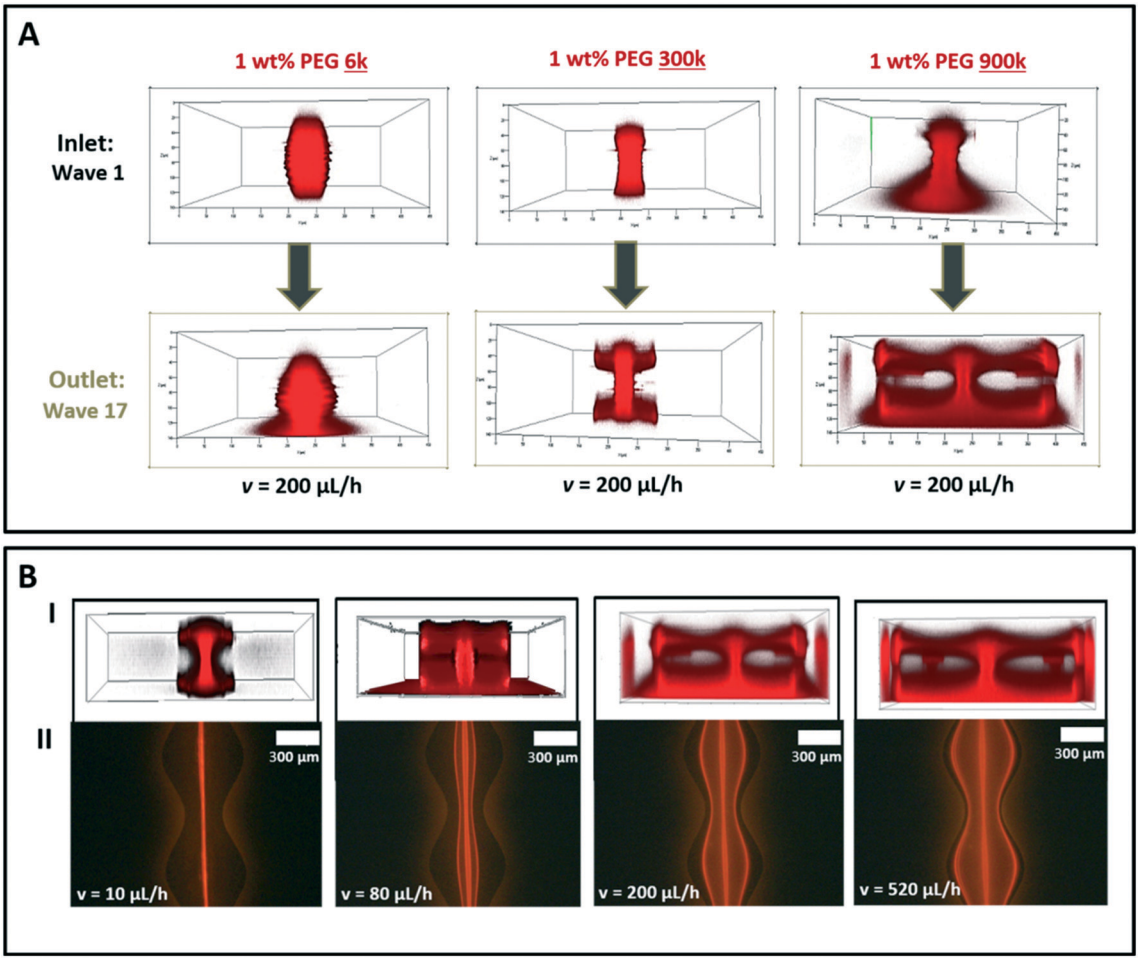

Fig. 3 (A) 3D-CLSM front view images at channel inlet and outlet of the flow profiles of the fluorescent dyed 1 wt% wormlike micelles in water within the standard sinusoidal channel (w = 250 μm, P = 800 μm, A = 150 μm, L = 100 μm) by using different molar mass of the non-Newtonian 1 wt% PEG-solution (M = 6000 g mol^{-1}, 300 000 g mol^{-1} and 900 000 g mol^{-1}) as 2D-focusing fluid at a constant flow velocity of v = 200 μL h^{-1} for all three inlets. (B) 3D-CLSM front view (I) as well as fluorescent top view (II) images of again the same wormlike micelles solution 2D-focused by the non-Newtonian 1 wt% PEG (900k) solution and this time varying flow rates between v = 10 and 520 μL h^{-1}.

which is typical for a polymer under good solution conditions. With a hydrodynamic volume of $V_h = \frac{4\pi}{3} R_h^3$, we can calculate the overlap concentration as $c^* = \frac{M}{N_A V_h}$, where N_A is Avogadro's number. With molecular weights of M = 6, 300, and 900 kg mol^{-1} we calculate c^* = 26, 1.6 and 0.74 wt%, such that the lowest molecular weight polyethylene glycol at a concentration of 1 wt% is clearly much below the overlap concentration, whereas the 300 kg mol^{-1} PEG is already close to the overlap concentration. The highest molecular weight 900 kg mol^{-1} PEG at a concentration of 1 wt% is clearly above the overlap concentration and thus in the semi-dilute concentration regime where adjacent polymer chains overlap and form a transient network of entangled polymer chains.

The 3D-focusing experiment clearly showed that wall-effects play a major role. The most dominant wall effect is a high wall shear rate, particularly for shear-thinning solutions. Because the channel height (h = 100 μm) is smaller than the mean channel width (w = 250 μm), the floor and ceiling wall shear rates are expected to have the most pronounced influence. With a average shear rate of $\dot{\gamma} = \frac{2v}{h}$ we obtain values of $\dot{\gamma}$ = 2.2, 18, and 133 s^{-1} for volumetric flow rates of 10, 80, and 600 μl h^{-1}. Thus already the average shear rates are of the same order of magnitude or higher compared to the inverse terminal relaxation time of a 1 wt% PEO solution (λ = 50 ms (ref. 30)), corresponding to Weissenberg numbers of Wi = $\lambda\dot{\gamma} > 1$, such that in the investigated shear rate regime visco-elastic responses are expected to be very pronounced close to the floor and ceiling of the microchannel wall.

A key to the understanding of the stream-splitting is according to our results in Fig. 1 and 2 the interplay between the non-Newtonian focusing fluid and the spatial modulation of the channel cross-section: there is no stream splitting of the suspension of deformable particles for a Newtonian focusing fluid in modulated channels and no stream splitting

with viscoelastic fluids in unmodulated, straight channels, but in combination of both.

Possible fluid inertia effects occur for larger values of the Reynolds number $\mathrm{Re} = \frac{\rho v D_h}{\eta}$, with ρ is the fluid density, η the shear viscosity, v the average velocity and $D_h = \frac{2wh}{(w+h)}$ the hydraulic diameter with w is the channel width and h is the channel height. This gives for our typical flow conditions, *i.e.* ρ = 1.0 g cm^{-3}, η = 0.001 Pa s, h = 100 μm, w = 250 μm, Q = 80…600 μl h^{-1} in the wide parts of the channel a Reynolds number in the range Re = 0.2…1.6 and in the narrow part Re = 0.5…3.75. Accordingly inertia effects are expected to be not dominating in agreement with our observations.

In the case of a Newtonian focusing fluid in Fig. 1 the slight particle depletion near the top and the bottom channel wall is in agreement with the expected lift forces in shear flows near walls[15–17] as well as with the particle-size dependent bulk migration of deformable particles.[11–14] The slight enhancement of the particle density for a shear thinning focusing fluid near the upper and bottom wall for a straight channel in Fig. 2 Ia is also consistent with the observed scenarios reported from previous experiments.[28]

The shear thinning focusing fluid leads to a flattening for the velocity profile near the center of the flow channel. Complementary, the magnitude of the shear gradient and its spatial variation is enhanced in a layers closer to the walls. Accordingly, wavy side-wall boundaries cause wavy streamlines mainly in the two shear thinning regions (STR) close to the upper and lower channel boundary, where the stream splitting is observed. These wavy streamlines are visualized by the wavy particle concentration in Fig. 2 Ib. The amplitude of the sinusoidal flow lines increases from zero at the channel center up to the modulated boundaries. In addition, the flow velocity along the flow lines in the STR's decreases with increasing distance from their centers, while the shear rate increases with distance from the centers of the STR's.

A linear shear flow is composed of a rational and an elongational flow, where the elongational component is oblique to the local stream direction. Accordingly, the mean shape of deformable particles in shear flow is elliptical and the major axis of this ellipse encloses an angle ψ with the local flow direction.[12–14] The dynamics of such deformed particles causes the lift force of soft particles away from flow-channel boundaries.[12–14] Flow fields in channels show nonlinear shear profiles, *i.e.* the shear rate changes across the finite size of the particles. Therefore deformable particles migrate across the local streamlines to ranges of smaller shear rates, *i.e.* in Poiseuille flows to the channel center.[15–17] In shear thinning fluids this migration may reverse and deformable particles migrate under certain condition also away from the center of straight channels,[37] but this effect is not dominating according to the results in Fig. 2. For small molecules like low molecular weight dyes cross-stream migration would not be expected.

Next we focus on particle migration in the STR's. The particle's inclination angle ψ has the same sign in both halves of a STR at the top and the bottom of the flow channel. The wavy streamlines in each half of the STR's cause an inhomogeneous, spatially modulated elongational flow. This leads to a spatial variation of the particle inclination angles ψ (without sign change). Accordingly, simultaneously the angle ψ and the shapes of flexible particles are different in each of both halves of a modulation wavelength. Therefore, the effects of a variation of the extensional flow acting across differently shaped particles and the overall drag forces cause different forces on the particles in each half of a modulation period. This difference leads to a net drag force per modulation-period and is mainly caused by geometrical factors. For particles in wavy streamlines of Newtonian fluids, this net force points always to the wavy channel boundaries and therefore away from the channel center.

This net force induced by the stream line modulations increases with modulation amplitudes and therefore with the distance from the channel center. Beyond a certain modulation amplitude this induced outward directed net migration outperforms the inward directed migration caused by the shear gradient variation across a particle, *i.e.* the direction of net-migration changes its sign beyond a certain distance from the channel center: the sign change never reaches the range near channel center with straight streamlines. As a result there is in modulated channels always a central particle stream left and therefore stream splitting.

This qualitative model is well in agreement with our experimental observations. The splitting effect is only observed in the high shear regions at the ceiling and floor of the microfluidic channels, where high shear rates lead to particle deformation and alignment. It is further only observed for sinusoidal channels, which are necessary to generate high extensional flow rates. These are highest at the beginning and at the end of each sine section. The extensional flow has different directions in the widening and in the narrowing section of each sine period, *i.e.* in the widening section in the first half of the sine period it is perpendicular to the flow direction, and in the narrowing section in the second half of the sine period it is parallel to the flow direction. This has been recently demonstrated in ref. 28. As the extensional force varies over the size of the particle, and because it has different directions with respect to the local orientation of the particles in the first and the second half of a sine period, it leads to a net migration over a certain distance towards the outer channel boundaries over each sine section. Higher flow rates, larger sine amplitudes and smaller sine periods lead to increased extensional forces and thus larger migration distances, which is well in agreement with our experiments.

2.4 Separation of different colloids

From our explanation it follows that the immersion of colloidal particles in a transient polymer network is a necessary

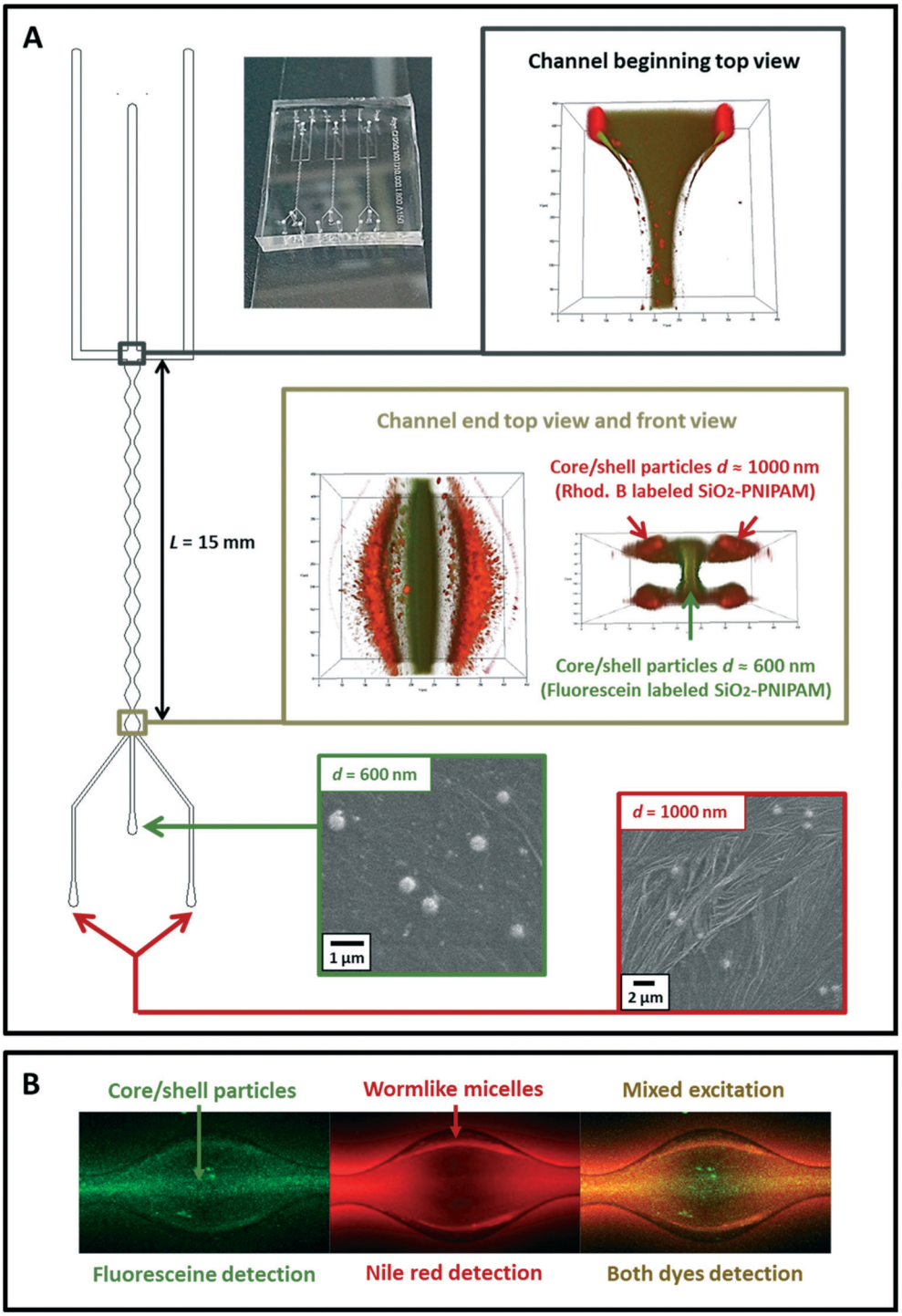

Fig. 4 (A) Sinusoidal microchip with three outlets for particle separation and 3D-CLSM images at channel cross and end. The device is used for non-Newtonian 1 wt% PEG (900k)-focusing of a bimodal distributed mixture of spherical SiO_2–PNIPAM core–shell particles with a diameter of d = 1000 nm and 600 nm. At the channel end, the two particle sizes are separated into a green center stream with fluorescein (FITC) labeled 600 nm particles and into four red sub-streams at the channel edges with rhodamine B (Rhod B) labeled 1000 nm particles. SEM images of the collected particle sizes are shown, whereby the bigger 1000 nm particles have been collected by the two side channels and the smaller 600 nm particles by the main channel. (B) Tripartite CLSM image at the channel end of the separation of a mixture of spherical core–shell particles d = 600 nm (FITC) and anisotropic wormlike micelles d = 20 nm (Rhod B) with polydisperse lengths focused by the same PEG-solution. Here, two detected emission wavelengths are shown, just FITC (left) and just Rhod B (mid) but also the overlay from both (right). In (A) we observe the separation of the bimodal distributed mixture of core–shell particles, and in (B) the separation of the wormlike micelles from the core/shell particles, corresponding to purities of >80% and >70%, respectively, as outlined in the ESI† (Fig. S7).

condition for stream splitting and separation. The combination of wormlike PI–PEO micelles in a PEO homopolymer network was chosen because of the mutual thermodynamic miscibility of the PEO polymer components. The miscibility can be affected by an increased viscosity, which prevents interdiffusion within the residence time in the microfluidic channels, and by thermodynamic effects such as depletion-induced demixing, which can particularly occur for mixtures of high molecular weight linear polymers and larger colloids. We therefore increased the concentration of the wormlike micelles from 1 over 5 to 10 wt% and investigated the streams under the standard flow conditions as outlined in Fig. 1. The streams were visualized by polarized light microscopy images at the entrance into the sinusoidal channel and at the last sine section. Whereas for the 1 wt% solution we observe a strong stream splitting and separation, for the 5 wt% solution the separation is less pronounced, and finally for the 10 wt% solution we observe no stream splitting at all, as visible in the ESI† (Fig. S5). This is related to the much larger viscosity of the concentrated wormlike micellar solution, but also indicates the expected depletion effect.

As cross-stream migration is an effective mechanism for particle separation, we investigated the possibility to separate colloids of different size in the splitting streams. We used a binary mixture of spherical silica–PNIPAM core–shell particles with a diameter of 600 nm, which were fluorescently labeled with fluorescein, and a diameter of 1000 nm which were labeled with rhodamine B. We used standard flow conditions (w = 400 μm, h = 100 μm, L = 1 cm, Q = 3 × 200 μL h^{-1}, 1 wt% PEG 900k) with a sinusoidal channel (P = 800 μm, A = 150 μm) that exits into three outlet channels as shown in Fig. 4. The location of the fluorescently labeled colloids could be followed by CLSM. Fig. 4A and S7A (ESI†) demonstrate that purities of >80% are achieved after the 12th sine section for each of the 600 and 1000 nm core/shell particles, and >70% for each of the wormlike micelles and 600 nm core/shell particles. The purities can be further increased by using channels with a larger number of sine sections.

3. Conclusion

We observed the splitting of streams of wormlike and spherical colloids into four substreams within sinusoidal microchannels. Splitting occurred when the streams were focused with a viscoelastic polymer solution. This effect could be used to separate spherical colloids of different size and spherical from wormlike colloids. By variation of the experimental conditions such as 2D- *vs.* 3D-focusing, straight *vs.* sinusoidal channels, sine period and amplitude, PEO molecular weight, Newtonian *vs.* non-Newtonian fluids we were able to reveal the essential conditions for the stream splitting effect which are caused by a combination of high extensional and shear rates in the shear-thinning zones of the modulated microchannels. This phenomenon can be generally used to separate colloidal and cellular particles according to their size.

4. Materials and methods

4.1 Fabrication of microfluidic devices

The microfluidic chip is initially fabricated by preparing a master device based on a Si wafer *via* optical lithography.[31] The microchannel structures are designed in AutoCAD 2013 (Autodesk) and printed on a mask foil with an UV-absorbent ink (JD Photo Data). A black and white drawing of the sinusoidal microchannel design is shown in Fig. 3A. Two different masters are finally used to produce the polydimethylsiloxane (PDMS) replicas for a 2D- respectively 3D-focusing chip design *via* soft lithography which is described in detail in the ESI.†[32–34] Afterwards, inlet ports are punched into the PDMS microchannels and interfaced with polyethylene (PE) tubes to be able to pump fluids into the devices by using high-precision syringe pumps (Nemesis system; Cetoni GmbH). For all carried out microfluidic experiments, the ratio of the flow rates between main channel and the two side channels was always constant with 1 : 1.

4.2 Preparation of block copolymer wormlike micelle solution

Polyisoprene$_{110}$-*b*-ethylene oxide$_{198}$ (PI_{110}–PEO_{198}) with a weight-averaged molar mass of M_w = 16 000 g mol^{-1} is synthesized by sequential living anionic polymerization, yielding an amphiphilic block copolymer with narrow polydispersity M_w/M_n = 1.02 (M_w and M_n are the weight- and number averaged molar mass). The detailed synthesis and characterization of PI_{110}–PEO_{198} is described in literature.[35] The polymer powder is dissolved in Millipore-quality water to a concentration of 20 wt% and by using an UltraTurrax T8 (IKA Werke GmbH) the solution was finally homogenized. Due to storing three weeks at room temperature the copolymer is able to swell enough in water and self-assemble wormlike micelles. The 20 wt% PI–PEO wormlike micelles stock solution is diluted with MilliQ water down to 1 wt%, 5 wt% respectively 10 wt% and filtered through a polytetrafluorethylene filter with 5 μm pore size. A cryo-transmission electron microscopy (cryo-TEM) image of the wormlike micelles is shown in the ESI† (see Fig. S2).

4.3 Preparation of core–shell particle dispersion

Core–shell particles with fluorescently labeled silica cores of approximately 100 nm in diameter and cross-linked poly-*N*-isopropylacrylamide (PNIPAM) shells were synthesized by seeded precipitation polymerization as previously reported.[36] The silica cores were either labeled with fluorescein or rhodamine B using the respective isothiocyanates of the dyes. These cores were then encapsulated in single-step[36] or sequential multi-step seeded polymerization[37] yielding core–shell particles with overall hydrodynamic diameter of approximately 600 and 1000 nm (swollen state conditions). The final core–shell particles were cleaned by repeated centrifugation and redispersion in water (at least three cycles). Fluorescence microscopy images of two selected samples that were studied in this work (fluorescein-labeled core, overall diameter of 600 nm as well as rhodamine B-labeled core, overall diameter of

1000 nm) are visible in the ESI† (Fig. S2). Furthermore, a scanning electron microscopy (SEM) image of the mixture of the SiO_2–PNIPAM core–shell particles in a non-Newtonian 1 wt% polyethylene glycol (PEG) aqueous solution is also shown in the ESI.†

4.4 3D-Confocal laser scanning microscopy

The confocal laser scanning microscopy analysis (CLSM) was carried out *via Z*-scan series of a Zeiss LSM 710 respectively a Leica TCS SP8 that was taken in the *x*–*y*–*z* mode and has been used to reconstruct 3D-images of the flow profiles along the whole microchannel. For the flow experiments, the laser was adjusted to the excitation wavelength of the used fluorescent dyes for the colloids. Thus, the argon laser was used with a wavelength of λ = 514 nm for Nile red respectively λ = 458 nm for fluorescein and the helium–neon laser with a wavelength of λ = 543 nm for rhodamine B. The colloid sample of the dyed wormlike micelles respectively of the core–shell particles was just injected *via* the middle channel, whereby the focusing fluid (water, glycerin or PEG) was always injected through the two side channels.

4.5 Fluorescence and polarization microscopy

Fluorescence and polarization microscopy was performed with an Axiovert S100 microscope in combination with an Axiocam HRc (Zeiss GmbH) to take pictures and movies. A mercury vapor lamp with specific filters was used to excite the right wavelength of all used fluorescent dyed colloids. The use of a polarization microscope with a quarter wave plate made it also possible to investigate the flow orientation of the colloids within the microchannels.

Conflicts of interest

There are no conflicts of interest to declare.

Acknowledgements

This work was financial supported by the German Ministry for Education and Research under Grant 05K13WC5 and the European Research Council Advanced Grant 291211. Prof. Dr. Matthias Karg acknowledges financial support from the German Research Foundation (DFG) *via* Emmy Noether programme.

References

1 P. Sajeesh and A. K. Sen, *Microfluid. Nanofluid.*, 2014, **17**, 1–52.
2 D. R. Gossett, W. M. Weaver, A. J. Mach, S. C. Hur, H. T. K. Tse, W. Lee, H. Amini and D. Di Carlo, *Anal. Bioanal. Chem.*, 2010, **397**, 3249–3267.
3 A. Karimi, S. Yazdi and A. M. Ardekani, *Biomicrofluidics*, 2014, **7**, 021501.
4 G. Segre and A. Silberberg, *Nature*, 1961, **189**, 209–210.
5 J. Zhang, S. Yan, D. Yuan, G. Alici, N.-T. Nguyen, M. Ebrahimi Warkiani and W. Li, *Lab Chip*, 2016, **16**, 10–34.
6 D. Di Carlo, *Lab Chip*, 2009, **9**, 3038–3046.
7 H. Amini, E. Sollier, W. M. Weaver and D. Di Carlo, *Proc. Natl. Acad. Sci. U. S. A.*, 2012, **109**, 11593–11598.
8 A. A. S. Bhagat, S. S. Kuntaegowdanahalli and I. Papautsky, *Microfluid. Nanofluid.*, 2009, **7**, 217–226.
9 S. C. Hur, N. K. Henderson-MacLennan, E. R. B. McCabe and D. Di Carlo, *Lab Chip*, 2011, **11**, 912–920.
10 D. Yuan, Q. Zhao, S. Yan, S.-Y. Tang, G. Alici, J. Zhang and W. Li, *Lab Chip*, 2018, **18**, 551.
11 S. Yang, S. S. Lee, S. W. Ahn, K. Kang, W. Shim, G. Lee, K. Hyun and J. M. Kim, *Soft Matter*, 2012, **8**, 5011–5019.
12 B. Kaoui, G. H. Ristow, I. Cantat, C. Misbah and W. Zimmermann, *Phys. Rev. E: Stat., Nonlinear, Soft Matter Phys.*, 2008, **77**, 021903.
13 S. K. Doddi and P. Bagchi, *Int. J. Multiphase Flow*, 2008, **34**, 966.
14 G. Coupier, B. Kaoui, T. Podgorski and C. Misbah, *Phys. Fluids*, 2008, **20**, 111702.
15 I. Cantat and C. Misbah, *Phys. Rev. Lett.*, 1999, **83**, 880.
16 U. Seifert, *Phys. Rev. Lett.*, 1999, **83**, 876.
17 M. Abkarian, L. Lartigue and A. Viallat, *Phys. Rev. Lett.*, 2002, **88**, 068103.
18 F. Del Giudice, S. Sathish, G. D'Avino and A. Q. Shen, *Anal. Chem.*, 2017, **89**, 13146–13159.
19 D. Li, X. Lu and X. Xuan, *Anal. Chem.*, 2016, **88**, 12303–12309.
20 C. Raghunath, G. W. Roland and G. Gerhard, *EPL*, 2010, **91**, 14001.
21 D. Steinhauser, S. Köster and T. Pfohl, *ACS Macro Lett.*, 2012, **1**, 541–545.
22 N. Xiang, Q. Dai and Z. Ni, *Appl. Phys. Lett.*, 2016, **109**, 134101.
23 C. Liu, C. Xue, X. Chen, L. Shan, Y. Tian and G. Hu, *Anal. Chem.*, 2015, **87**, 6041–6048.
24 T. Go, H. Byeon and S. J. Lee, *Sci. Rep.*, 2017, **7**, 41162.
25 C. F. Hewitt and J. S. Marschall, *J. Fluid Mech.*, 2010, **660**, 258–281.
26 S. Cha, K. Kang, J. B. You, S. G. Im, Y. Kim and J. M. Kim, *Rheol. Acta*, 2014, **53**, 927–933.
27 D. Yuan, J. Zhang, S. Yan, C. Pan, G. Alici, N. T. Nguyen and W. H. Li, *Biofluidmechanics*, 2015, **9**, 044108.
28 M. Trebbin, D. Steinhauser, J. Perlich, A. Buffet, S. V. Roth, W. Zimmermann, J. Thiele and S. Förster, *Proc. Natl. Acad. Sci. U. S. A.*, 2013, **110**, 6706–6711.
29 K. Devanand and J. C. Selser, *Macromolecules*, 1991, **24**, 5943–5947.
30 S. Mukherjee and K. Sarkar, *Phys. Fluids*, 2014, **26**, 103102.
31 N. T. Nguyen and S. Wereley, *Fabrication Techniques for Microfluidics*, Artech House, Norwood, MA, 2002.
32 G. M. Whitesides and Y. Xia, *Annu. Rev. Mater. Sci.*, 1998, **28**, 153–184.
33 S. R. Quake and A. Scherer, *Science*, 2000, **290**, 1536–1540.
34 J. C. McDonald, D. C. Duffy, J. R. Anderson, D. T. Chiu, H. Wu, O. J. A. Schueller and G. M. Whitesides, *Electrophoresis*, 2000, **21**, 27–40.
35 S. Förster and E. Krämer, *Macromolecules*, 1999, **32**, 2783–2785.
36 A. Rauh, M. Rey, L. Barbera, M. Zanini, M. Karg and L. Isa, *Soft Matter*, 2017, **13**, 158–169.
37 S. A. Vasudevan, A. Rauh, L. Barbera, M. Karg and L. Isa, *Langmuir*, 2018, **34**, 886–895.